Vesicles as reactors of nanoparticles: an anomalous small-angle X-ray scattering study of the domains rich in copper ions

Attila Bóta,[a]* Zoltán Varga[a] and Günter Goerigk[b]

[a]Department of Physical Chemistry, Budapest University of Technology and Economics, Műegyetem rkp 3, H-1521 Budapest, Hungary, and [b]Institute of Solid State Physics, Research Centre Jülich, D-52425 Jülich, Germany. Correspondence e-mail: abota@mail.bme.hu

The formation of copper hydroxide and copper oxide particles in the gaps among the stacks of multilamellar vesicles is described, illustrating a new pathway in the preparation of nanometre-scale particles. The *in situ* structural characterization of both the solid particles and the vesicles as a reaction medium was performed in the initial and final states of the process by using anomalous small-angle X-ray scattering (ASAXS) and freeze-fracture methods. The ASAXS method provides a description of the particle-size distribution of the copper nanoparticles, in spite of the fact that they are present in low concentration. This method allows the particle formation and growth to be monitored throughout the whole time range of the synthesis.

1. Introduction

The application field of nanoparticles has expanded enormously (Valden *et al.*, 1998; Huynh *et al.*, 2002; Bell, 2003). A number of methods are known to produce nanoparticles which require different reaction mediums (Dékány *et al.*, 1995; Caponetti *et al.*, 2003; Pedone *et al.*, 2005; Shi *et al.*, 2004). Among them the ordered organic matrixes must be mentioned: Langmuir–Blodget films, microemulsions and unilamellar vesicles (Fendler, 1984, 1987; Mann *et al.*, 1986; Zhu *et al.*, 1992; Pileni *et al.*, 1992; Korgel & Monbouquette, 2000). Unilamellar vesicles (or liposomes) consisting of natural or artificial amphiphilics are ideal systems for the synthesis of nanoparticles because the versatility of their double lipid layer makes size and shape modifications possible. The core of the unilamellar vesicles as an aqueous nanoreactor provides a place for the chemical reaction resulting in solid nanoparticles. Besides the unilamellar vesicles, their multilamellar forms can also be used for the synthesis of nanoparticles as shown in this work.

Generally, the salts of bivalent metal ions (Ca, Cu, Zn, Cd *etc.*) cause drastic destruction of the periodic layer arrangement of vesicles, even in small concentrations (Binder & Zschörnig, 2002). The structural and the morphological features of the location of copper ions were studied in the dipalmitoylphosphatidylcholine (DPPC)–water system [20% lipid/(lipid + water) *w/w*] at low concentration (0.01 copper/lipid molar ratio) using small-angle X-ray scattering (SAXS) and anomalous small-angle X-ray scattering (ASAXS). It was concluded that only the ASAXS method can provide information about the structural features of the domains rich in copper ions, which are mainly located in the large domains between the lamellae and only partly in the characteristic periodic water shells of the liposomes (Bóta *et al.*, 2002). Moreover, the local structures induced by the copper ions were visualized by a freeze-fracture technique. Some stacks of lamellae of vesicles are open and gaps appear between them. The characteristic size of the gaps correlates with the value deduced by ASAXS for the size of the domains rich in copper ions. The domains formed between the multilamellar vesicles can be utilized for the preparation of nanoparticles, serving as a new pathway in their production.

2. Experimental

2.1. Sample preparation

Synthetic high-purity (more than 99%) 1,2-dipalmitoyl-*sn-glycero*-3-phosphatidylcholine (DPPC) and copper chloride (CuCl$_2$·2H$_2$O) were obtained from Avanti Polar Lipids (USA) and from Merck (Germany), respectively. The chemicals were used without any further purification. The 20% *w/w* DPPC system (with 0.01 and 0.05 Cu/DPPC molar ratio) was made from the pure lipid and CuCl$_2$·2H$_2$O solution (3.4 and 17 mmol dm^{-3}) using a neutral Tris buffer system (50 mmol dm^{-3}) by simple mixing. In the first stage of the procedure the samples were kept at 323 K for 10 min then vortexed intensively and quenched to 277 K. This process was repeated at least twenty times to get a homogeneous liposome system. In the second stage, for the synthesis of Cu(OH)$_2$, NaOH was used in an over-stoichiometric amount (20 mol% excess). In the third stage of the synthesis, the sample was heated up to 353 K then cooled down to 300 K; this treatment was repeated three times.

2.2. Methods

For the X-ray measurements, the samples were transferred into thin-walled [Plexiglas, 0.25 mm thick, without significant small-angle scattering (Röhm, Darmstadt, Germany)] 'sandwich' sample holders. Each sample holder was closed in a sample-holder block made of aluminium. This block also had the same Plexiglas windows. Between the windows of the sample holder and the sample-holder block, thermostated water (0.1 mm thick) was circulated to provide precise incubation at the desired temperatures.

SAXS and ASAXS measurements were carried out at the JUSIFA (B1) beamline at HASYLAB (DESY, Hamburg, Germany) in the regime of the modulus of the scattering vector q [$q = (4\pi/\lambda)\sin\Theta$, where λ is the wavelength and 2Θ is the scattering angle] from 0.006

up to 0.5 Å^{-1} (Haubold *et al.*, 1989). The selected energies were 8510, 8972, 8979 and 8984.5 eV, *i.e.* close to the *K* edge of copper (8979 eV, measured by the absorption of both copper and CuCl$_2$ solution). In the case of the DPPC/CuCl$_2$/H$_2$O system a chemical shift of about 5 eV was observed and in the presence of Cu(OH)$_2$ and CuO significant changes were not observed.

For freeze fracture, a quantity of about 200 mg of the lipid system was prepared in a small, covered glass vial. The gold sample holders used for the freeze fracture were also preincubated at 300 K. Droplets of 1–2 µl were pipetted onto the gold holders, which were then immediately plunged into partially solidified Freon for 20 s freezing and then placed and stored in liquid nitrogen. Fracturing was carried out at 173 K in a Balzers freeze-fracture device (Balzers AG, Liechtenstein). The fractured faces were etched for 30 s at 173 K. The replicas, prepared by platinum–carbon shadowing, were cleaned with a solution of surfactant and washed in distilled water. The replicas were picked up from pure water on 200 mesh copper grids. The electron micrographs were taken in a Jeol JEM-100 CX II electron microscope (Jeol, Japan).

3. Results and discussion

3.1. Copper-ion effect on the regularity of vesicles

The bivalent copper ions cause significant destruction of the layer arrangement of multilamellar vesicles. This effect appears already at low concentrations (0.01 Cu/lipid molar ratio), but the presence of a buffer system results in a regular formation of the vesicles, as can be concluded from the SAXS pattern showed in Fig. 1. The further increase in copper concentration induces severe destruction in the vesicles as observed in the case of the 0.05 Cu/lipid molar ratio. Only two peaks appear in the one-dimensional SAXS curve at 0.05 Cu/lipid molar ratio: one of them is an intense diffuse reflection, the other one is relatively small. The extremely broadened first one can be interpreted as a sum of the broadened first and second Bragg reflections, indicating a weak correlation between the layers. The reduced number of Bragg reflections hinders the reconstruction of the characteristic electron density profile of the system, whereby the positions of copper ions inside the hydrated double layers cannot be determined (Tristram-Nagle & Nagle, 2004). The broadening of Bragg reflection profiles, however, can be explained by the paracrystalline
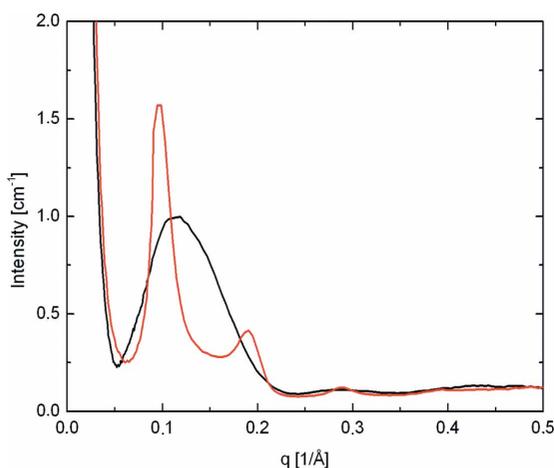
theory (PT) (Guinier, 1963). The scattering intensity of stacks of lamellae is given by the multiplication of two terms (Zhang *et al.*, 1994; Pabst *et al.*, 2000, 2003),
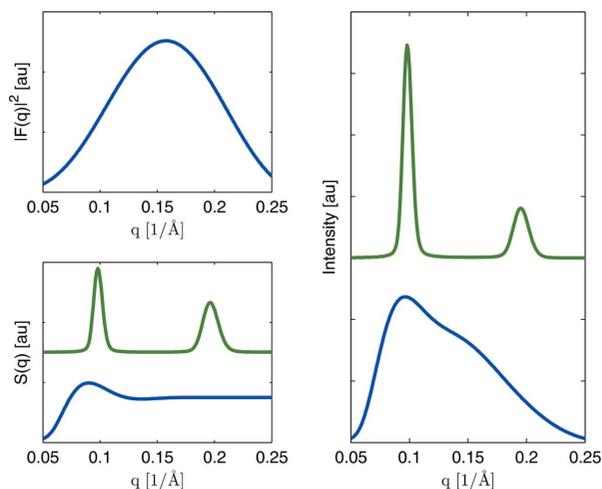
$$I(q) = S(q)\big|F(q)\big|^2/q^2, \qquad (1)$$

where $S(q)$ is the structure factor for the one-dimensional layer arrangement and $F(q)$ is the form factor of each double-layered unit without any additional diffuse scattering term. Taking into account the second type of disorder (stacking disorder, small variation in the bilayer), the structure factor is described by

$$S_{PT}(q) = N + 2\sum_{k=1}^{N-1}(N-k)\cos(kqd)\exp(-k^2q^2\Delta^2/2), \qquad (2)$$

where N is the number of layers, d is the periodicity, k is an integer and Δ is the mean fluctuation of each layer in the stacks. A simple model calculation was applied to interpret the formation of the Bragg reflections. By changing the Δ parameter of the structure factor, the characteristic scattering curves were reconstructed for two extremes, corresponding to the lower and higher copper concentrations, to achieve real cases like those in the systems having 0.01 and 0.05 Cu/lipid ratios. In the model calculations the same form factors were used. The measured and the simulated intensity curves shown in Figs. 1 and 2, respectively, show high similarity explaining the concentration effect on the layer arrangement. It can be concluded that at higher concentration the inhomogeneous location of copper ions results in the weakly correlated layer packing of vesicles in spite of the presence of a buffer system. The strong scattering intensities of both systems in the q range smaller than 0.05 Å^{-1} are the consequence of the domain formation in the size range of several tens of nanometres.

The application of ASAXS provides an opportunity for determining the local domain structures that contain copper ions. The method was first introduced for protein crystallography (Phillips *et al.*, 1977), for wide-angle diffraction of membranes (Stamatoff *et al.*, 1982) and for diluted macromolecules (Stuhrmann, 1985). De Robbilard *et al.* (2001) and very recently Goerigk *et al.* (2004) described spherical polyelectrolyte brushes by the ASAXS scattering of the counterions. Richardsen *et al.* (1996) reported that in multilamellar vesicle systems the location of rubidium ions can be followed by the difference of the electron density profiles using the ASAXS

Figure 1
One-dimensional SAXS patterns of the DPPC/water (20% *w/w*) multilamellar vesicles doped with copper ions (CuCl$_2$) at two different concentrations. One of the curves exhibits sharp Bragg reflections, while the other one has a broadened diffuse peak, corresponding to 0.01 and 0.05 Cu/DPPC ratios, respectively.

Figure 2
The representation of the shapes of the Bragg reflections of the SAXS curves within the paracrystalline theory. The same form factor, $F(q)$, and different structure factors, $S(q)$, with $\Delta = 2$ and 20 Å were used in the simulations.

technique. The theory of this method is based on the energy (E) dependence of the scattering factors f of the different atoms, in our case copper, which are conveniently written as complex quantities

$$f_{Cu}(E) = f_{0,Cu} + f'_{Cu}(E) + if''_{Cu}(E). \qquad (3)$$

Consequently the scattering amplitude of the system can be described as the sum of the terms corresponding to the energy-independent (A) and -dependent $[(f' + if'')V]$ ones. In this case the total intensity contains three terms:

$$I(q, E) = \{A(q)^2 + 2f'(E)A(q)V(q) + [f'^2(E) + f''^2(E)]V(q)^2\}\frac{S(q)}{q^2}, \qquad (4)$$

where V is the scattering of the resonant copper ions. The ASAXS study requires measurements at two different energies at least; at an energy close to the absorption edge and at another far away from it. The difference of two ASAXS curves measured at the two different energies (known as separated ASAXS curves) is characteristic of the structure of the domains containing copper ions, shown in Fig. 3. In the separated curves, a contrast effect appears at nearly the same interval of the modulus of the scattering vector as the displacement of the intense broadened Bragg reflection observed in each ASAXS curve. The appearance of this peak indicates that the copper ions are also located in a layer arrangement corresponding to aqueous shells of destroyed liposomes. These separated ASAXS curves, however, contain two terms, the cross and the 'pure resonant' terms as described by

$$\begin{aligned} \Delta I(q, E_1, E_2) &= I(q, E_1) - I(q, E_2) \\ &= \{2[f'(E_1) - f'(E_2)]A(q)V(q) + [f'^2(E_1) - f'^2(E_2) \\ &+ f''^2(E_1) - f''^2(E_2)]V^2(q)\}\frac{S(q)}{q^2}. \end{aligned} \qquad (5)$$

Both of the terms contain the 'pure resonant' term of copper as a factor for multiplication and, therefore, the local layered presence of the copper ions is obvious. To obtain more quantitative information about the location of the copper ions, the detection of ASAXS curves is required at three different energies. Unfortunately, these measurements did not result in sufficient separation between the terms because of the relatively high error ranges of the intensity curves.
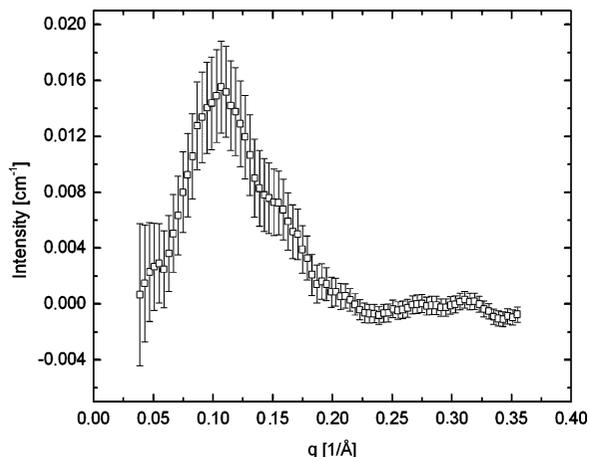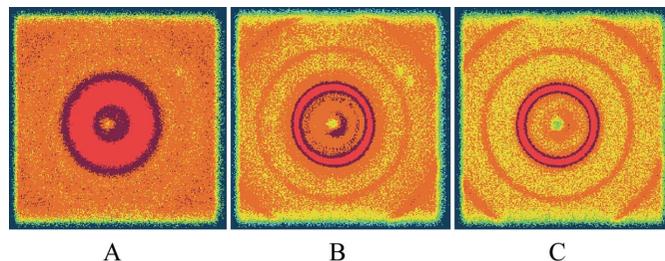
Figure 4
Changes in the SAXS patterns of the DPPC/water system during the synthesis of copper nanoparticles corresponding to the three stages of the formation of the copper-ion containing domains. A: the beginning state: large domains rich in copper embedded between the layers of the vesicles, doped with CuCl$_2$; B: domains rich in copper in the form of Cu(OH)$_2$, which are separated from the stacks in a predominantly gel (L$_{\beta'}$) phase; C: domains rich in copper in the form of CuO, which are separated from the stacks in the L$_I$ phase.

After adding NaOH solution as a reagent to the system, the two-dimensional scattering pattern is significantly changed: instead of a single broadened ring, several narrow ones occurred, clearly showing the recombination of the regular arrangement of the multilamellar system. The scattering patterns of each stage of the preparation are shown in Fig. 4. The position of the first Bragg reflection corresponds to a layer periodicity of 61.6 Å. After the heating process the Bragg rings became narrower and their positions were shifted to larger values of the modulus of the scattering vector, corresponding to a periodicity of 43.3 Å as presented in the one-dimensional scattering curve in Fig. 5. This small value of the characteristic distance indicates the formation of the interdigitated gel phase (L$_I$), where the hydrocarbon chain regions of the the double-lipid layers are embedded into each other. The SAXS patterns are informative about the changes in the matrix, but the formation of the solid particles consisting of copper ions can be followed by the ASAXS method. The separated ASAXS curves indicate that after adding NaOH to the system, yielding copper hydroxide solid particles, the contrast effect is very low and it is the same as the error range. From other side, the precipitation must have occurred outside the stacks of multilayers because of the appearance of sharp Bragg rings. After the heating process, no contrast effect appears in the scattering regime of the Bragg reflections, but there is a detectable one (~1%) at the begin-
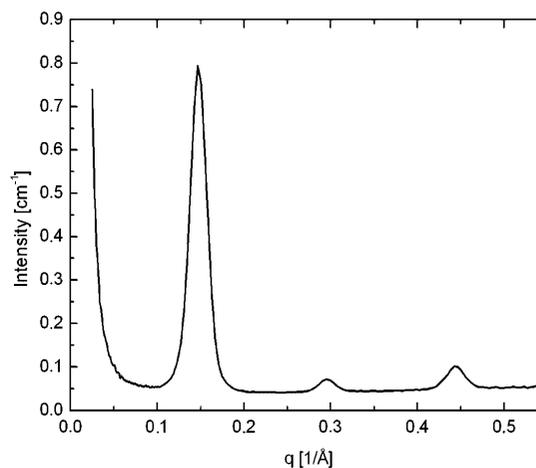

Figure 3
Separated ASAXS curves of the DPPC/water vesicles doped with copper ions with 0.05 Cu/DPPC molar ratio in the intense Bragg reflection regime of the modulus of the scattering vector.

Figure 5
One-dimensional SAXS pattern of the DPPC/water (20% w/w) system after the formation of an interdigitated phase (induced by heat treatment) and the separation of the domains containing CuO particles.

ning of the scattering curve. In this third treatment process two different changes occurred; the copper particles are transformed into copper oxide by a change in their size distribution and a phase transition in the reaction medium. However, we can not preclude the presence of copper hydroxide particles. After measuring at three different energies, the determination of the scattering of the copper particles is possible by using the following equation, supposing that there is no correlation between the particles (Goerigk *et al.*, 2004):

$$V_{Cu}^2(q) = \frac{1}{C(E_1, E_2, E_3)} \left[\frac{\Delta I(q, E_1, E_2)}{f'(E_1) - f'(E_2)} - \frac{\Delta I(q, E_1, E_3)}{f'(E_1) - f'(E_3)} \right],$$

$$C(E_1, E_2, E_3) = f'(E_2) - f'(E_3) + \frac{f''^2(E_1) - f''^2(E_2)}{f'(E_1) - f'(E_2)} - \frac{f''^2(E_1) - f''^2(E_3)}{f'(E_1) - f'(E_3)}.$$

(6)

This 'pure resonant' term is shown in Fig. 6. From that, by assumption of a log-normal function, the size distribution of copper oxide was fitted using the expressions
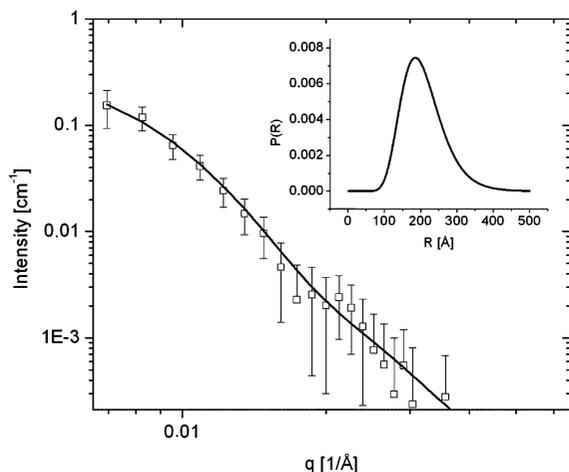
$$V_{Cu}^2(q) = const \int_0^\infty P(R) \left\{ \frac{4\pi R^3}{3} \frac{3[\sin(qR) - qR\cos(qR)]}{(qR)^3} \right\}^2 dR,$$

$$P(R) = \frac{1}{\sqrt{2\pi}} \frac{1}{\sigma R} \exp\left[-\frac{\ln^2 R/R_0}{2\sigma^2} \right],$$
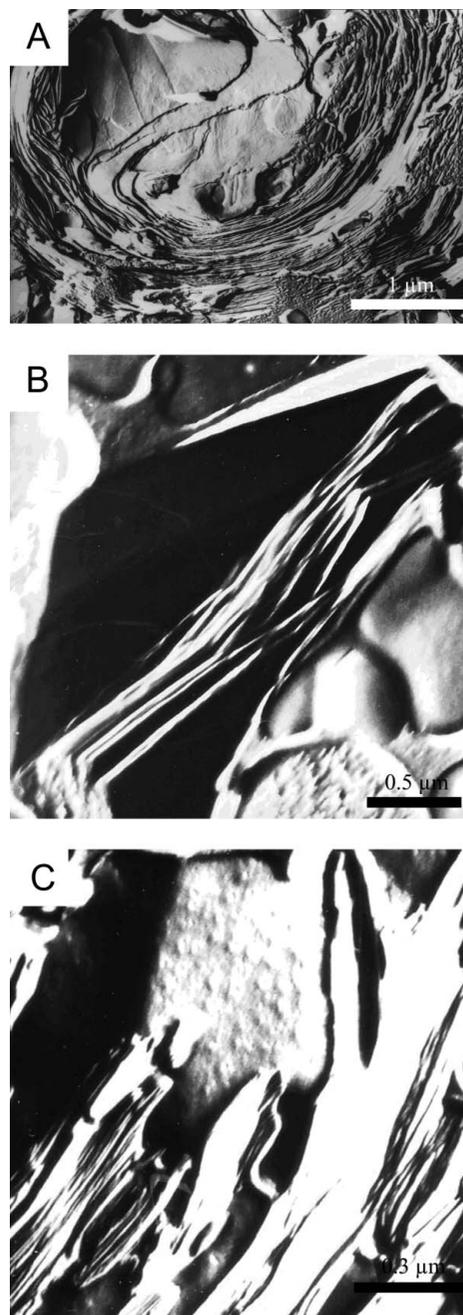
(7)

and is presented as an inset to Fig. 6.

3.2. Morphological changes in the reaction medium

Freeze fracture is a unique method for the direct visualization of the surface morphology of the vesicles (Meyer & Richter, 2001). In this section we present some electron micrographs taken at the three stages of the preparation process. Firstly, the surface morphology of a giant vesicle containing CuCl$_2$ (Cu/DPPC = 0.05, buffer system, pH = 7.4) broken through completely, at the start of the synthesis of the solid particles, is shown in Fig. 7A. The irregularity of the multi-lamellar arrangement is evident and the direct visual information is in full agreement with the interpretation of the weak correlation within the paracrystalline theory. Some stacks of lamellae are open and gaps are formed between them, presumably as a consequence of domains rich in copper ions, as interpreted in our previous study for the same system also containing copper ions (0.01 Cu/DPPC molar ratio)

Figure 7
Changes in the surface morphologies of the DPPC/water system during the synthesis of copper nanoparticles corresponding to the three stages of the formation of the copper-ion-containing domains (their SAXS patterns are shown in Fig. 4). A: the first state with a destroyed layer arrangement in the giant vesicle broken through entirely; B: stack of lamellae and undefined morphology in the surrounding medium; C: stacks of lamellae with grained domains in which each grain extends to 300–400 Å.

(Bóta & Klumpp, 2005). In Figs. 7B and C, the typical centro-symmetrical vesicles can not observed, only macroscopically unoriented stacks of parallel layers appear which are separated from the medium with undefined morphologies. The existence of closely packed layers clearly gives an explanation for the sharper rings in the SAXS patterns shown in Figs. 4B and C. Moreover, in the third stage of synthesis, where the formation of copper oxide particles is supposed, the medium exhibits a grained surface. The grains extend

Figure 6
The pure resonant term of the domains of CuO particles. The inset represents the size distribution of these domains.

between 300–400 Å, in good agreement with the size distribution observed by the ASAXS method.

4. Conclusion

The water shells of multilamellar vesicles can be used as reaction compartments for the synthesis of nanoparticles. The precursors of particles are dispersed inhomogeneously in the vesicle system forming domains between the stacks of lamellae. After adding an appropriate reagent to the system nanoparticles can be prepared. If the reagent induces another phase in the vesicles, the formation of larger particles is expected. Besides monitoring the changes in reaction medium, the ASAXS method also provides 'in situ' structural characterization of nanoparticles during the synthesis. The latter advantage of the ASAXS method indicates a unique use of synchrotron radiation and the simultaneous monitoring of nanoparticle formation becomes possible during the entire procedure of synthesis.

References

Bell, A. T. (2003). *Science*, **299**, 1688–1691.
Binder, H. & Zschörnig, O. (2002). *Chem. Phys. Lipids*, **115**, 39–61.
Bóta, A., Goerigk, G., Haubold, H.-G., Vad, T. & Subklew, G. (2002). *Annual Report*, Desy/Hasylab.
Bóta, A. & Klumpp, E. (2005). *J. Colloids Surfactants A*, **265**, 124–130.
Caponetti, E., Pedone, L., Martino, D. C., Panto, V. & Liveri, V. T. (2003). *Mater. Sci. Eng. C*, **23**, 531–539.
Dékány, I., Turi, L., Tombácz, E. & Fendler, J. H. (1995). *Langmuir*, **11**, 2285–2292.
Fendler, J. H. (1984). *Science*, **223**, 888–894.
Fendler, J. H. (1987). *Chem. Rev.* **87**, 877–899.
Goerigk, G., Schweins, R., Huber, K. & Ballauff, M. (2004). *Europhys. Lett.* **66**, 331–337.
Guinier, A. (1963). *X-ray Diffraction*. San Francisco: Freeman.
Haubold, H.-G., Gruenhagen, K., Wagener, M., Jungbluth, H., Heer, H., Pfeil, A., Rongen, H., Brandenburg, G., Moeller, R., Matzerath, J., Hiller, P. & Halling, H. (1989). *Rev. Sci. Instrum.* **60**, 1943–1946.
Huynh, W. U., Dittmer, J. J. & Alivisatos, A. P. (2002). *Science*, **295**, 2425–2427.
Korgel, B. A. & Monbouquette, H. G. (2000). *Langmuir*, **16**, 3588–3594.
Mann, S., Hannington, J. P. & Williams, R. J. P. (1986). *Nature (London)*, **324**, 565–567.
Meyer, H. W. & Richter, W. (2001). *Micron*, **32**, 615–644.
Pabst, G., Koschuch, R., Pozo-Navas, B., Rappolt, M., Lohner, K. & Laggner, P. (2003). *J. Appl. Cryst.* **36**, 1378–1388.
Pabst, G., Rappolt, M., Amenitsch, H. & Laggner, P. (2000). *Phys. Rev. E*, **62**, 4000–4009.
Pedone, L., Caponetti, E., Leone, M., Militello, V., Pantó, V., Polizzi, S. & Saladino, M. L. (2005). *J. Colloid Interf. Sci.* **284**, 495–500.
Phillips, J. C., Wlodawer, A., Goodfellow, J. M., Watenpaugh, K. D., Sieker, L. C., Jensen, L. H. & Hodgson, K. O. (1977). *Acta Cryst.* A**33**, 445–455.
Pileni, M. P., Motte, P. & Petit, C. (1992). *Chem. Matter*, **4**, 338–345.
Richardsen, R., Vierl, U., Cevc, G. & Fenzl, W. (1996). *Europhys. Lett.* **34**, 543–548.
Robbilard, Q. de, Guo, X., Dingenouts, N. & Ballauff, M. (2001). *Macromol. Symp.* **164**, 81–90.
Shi, J., Quin, Y., Wu, W., Li, X., Guo, Z.-X. & Zhu, D. (2004). *Carbon*, **42**, 423–460.
Stamatoff, J., Eisenberger, P. E., Blasie, J. K., Pachence, J. M., Tavormina, A., Erecinska, M., Dutton, P. L. & Brown, G. S. (1982). *Biochim. Biophys. Acta*, **679**, 177–187.
Stuhrmann, H. B. (1985). *Adv. Polym. Sci.* **67**, 123–163.
Stuhrmann, H. B., Goerigk, G. & Munk, B. (1991). *Anomalous X-ray Scattering*. In *Handbook on Synchrotron Radiation*, Vol. 4, edited by S. Ebashi, M. Koch & E. Rubenstein. Netherlands: Elsevier.
Tristram-Nagle, S. & Nagle, J. F. (2004). *Chem. Phys. Lipids*, **127**, 3–14.
Valden, M., Lai, X. & Goodman, D. W. (1998). *Science*, **281**, 1647–1650.
Zhang, R., Suter, R. M. & Nagle, J. F. (1994). *Phys. Rev. E*, **50**, 5047–5060.
Zhu, R., Min, G. W. & Wei, Y. J. (1992). *J. Phys. Chem.* **96**, 8210–8211.